Electron Transporting Perylene Diimide-Based Random Terpolymers with Variable Co-Monomer Feed Ratio: A Route to All-Polymer based Photodiodes

Journal:	*Macromolecules*
Manuscript ID	ma-2021-02159x.R1
Manuscript Type:	Article
Date Submitted by the Author:	12-Dec-2021
Complete List of Authors:	Aivali, Stefania; University of Patras School of Natural Sciences, Chemistry Yuan, Peisen; CIC nanoGUNE, Panidi, Julianna ; University of Southampton Georgiadou, Dimitra; University of Southampton, Zepler Institute for Photonics and Nanoelectronics Prodromakis, Themis; Nano Group, Nanofabrication Centre,, Electronics and Computer Science Faculty of Physical Sciences and Engineering Kallitsis, Joannis; University of Patras School of Natural Sciences, Chemistry Keivanidis, Panagiotis; Cyprus University of Technology, Department of Mechanical Engineering and Materials Science and Engineering Andreopoulou, Aikaterini; University of Patras, DEPARTMENT OF CHEMISTRY

Electron Transporting Perylene Diimide-Based Random Terpolymers with Variable Co-Monomer Feed Ratio: A Route to All-Polymer based Photodiodes

Stefania Aivali[†], Peisen Yuan[§], Julianna Panidi[#], Dimitra G. Georgiadou[#], Themis Prodromakis[#], Joannis K. Kallitsis[†, ¥], Panagiotis E. Keivanidis[§] and Aikaterini K. Andreopoulou[†,¥*]*

[†] Department of Chemistry, University of Patras, University Campus, Rio-Patras, GR26504, Greece.

[¥] Foundation for Research and Technology Hellas/Institute of Chemical Engineering Sciences (FORTH/ICE-HT), Platani Str., Patras, GR26504, Greece

[§] Device Technology and Chemical Physics Laboratory, Department of Mechanical Engineering and Materials Science and Engineering, Cyprus University of Technology, 45 Kitiou Kyprianou str., Limassol 3041, CYPRUS

[#] Centre for Electronics Frontiers, Electronics and Computer Science, University of Southampton, Highfield Campus, University Road, Building 53 (Mountbatten), Southampton SO17 1BJ, United Kingdom

for Table of Contents use only

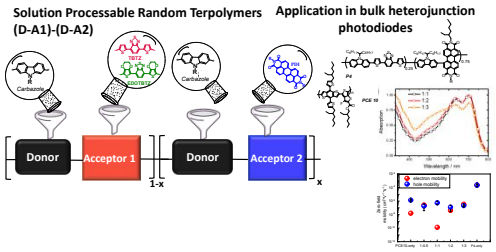

KEYWORDS: conjugated polymers, random terpolymer acceptors, perylene diimide, photodetectors, all-polymer solar cells, trap-limited charge recombination

ABSTRACT

A route towards processable n-type terpolymers is presented herein based on the random donor–acceptor–donor–acceptor (D–A1)-(D–A2) molecular configuration. Carbazole is utilized as the electron donating unit (D) combined with perylene diimide (PDI) as the first electron acceptor (A1) and either one of two different benzothiadiazole (BTZ) derivatives (di-thienyl substituted-BTZ and di-3,4-ethylenedioxythienyl substituted-BTZ) as the second electron accepting unit (A2). Increasing the content of the PDI co-monomer resulted in terpolymers of higher molecular weights, enhanced solubility and stronger n-type character. The physicochemical properties of the random PDI-Cz-BTZ derivatives are fine-tuned based on the feed ratio of the co-monomers.

Photodiode devices were demonstrated, having photoactive layers composed of the rich in PDI terpolymer, namely P4 having a 75% PDI content, and the PCE10 electron donor, under various ratios. For a range of P4 blend compositions UV-Vis spectroscopy confirmed the strong absorption of the blend films across the 350 – 800 nm spectral region, and AFM imaging verified their low surface roughness. The study of the electro-optical device properties identified the 1:2 blending ratio as the optimum PCE10:P4 combination for maximum charge photogeneration efficiency. Despite the relatively deep LUMO energy of the n-type P4 terpolymer (E_{LUMO}= -4.04 eV), trap-limited charge recombination losses were found to limit the PCE10:P4 photodiodes performance. Unipolar devices of the P4-alone exhibited hole and electron mobility values of 2.2 $\times 10^{-4}$ $cm^2V^{-1}s^{-1}$ and 6.3 $\times 10^{-5}$ $cm^2V^{-1}s^{-1}$, respectively.

1. Introduction

Donor-acceptor conjugated copolymers have been extensively studied over the past decade as prominent organic polymers for polymer solar cells (PSCs)[1,2,3]. Copolymers combining one electron-rich and one electron-poor unit, alternating in the polymer chain, create a "push–pull" effect[4,5] that results in reduced bandgap and absorption of more photons from the solar spectrum, affording record efficiencies in PSCs[6,7,8]. Outstanding progress has been made owing to innovations in synthetic methodology and materials design, which have led to a vast library of π-conjugated oligomeric and polymeric semiconductors with tunable functionality[9,10]. The molecular design, including the combination of different donor and acceptor units and/or side chains in the polymer backbone, provides the opportunity to efficiently tune the absorption characteristics and control the electrochromic properties[11,12].

Lately, this strategy has been enriched with the development of random terpolymers as a promising route for solution-processed PSCs[13,14,15]. Random terpolymers contain two donors and one acceptor (D1–A)-(D2–A) or one donor and two acceptors (D–A1)-(D–A2) in the polymer backbone. With the incorporation of a third moiety with absorption spectrum complementing these of the other two units, broader light absorption could be achieved facilitating the harvesting

of more photons. Additionally, their random structure imparts processability, providing miscibility, control of the crystallinity and the opportunity to fine-tune the energy levels in the polymeric structure[16,17,18,19]. The high processability and suppressed aggregation that random copolymers endow were highlighted by Son *et al.* constructing polymer solar cells with 1 cm^2 active area based on a D1-A-D2-A terpolymer blended with $PC_{71}BM$ with PCE up to 9.4%[20]. Most recently, Jenekhe *et al.* developed random copolymers acting as non-fullerene acceptors with PCEs up to 10.1% without using any additive in the active layer's blend, underlining the improved nanophase morphology that random copolymers provide[21]. In the field of electron acceptors, n-type semiconducting small molecules are rising as the most prominent materials for the active layer and among them perylene diimide (PDI) derivatives have exhibited the most promising features. The class of PDI electron acceptors is highly favorable; PDIs are easily processable by most organic solvents, their absorption profile can be tuned on demand via simple chemistry, and their cost is lower than of fullerene derivatives. Most importantly, the LUMO energy level of molecular PDI derivatives is deeper than the electron trapping sites that have been identified as the universal bottleneck for trap-free electron transport in organic semiconductors[22,23]. Non-planar structures combining different organic building blocks have

been investigated in order to overcome the intense self-aggregation of PDI derivatives that lead to oversized domains and ultimately poor photovoltaic performance[24,25]. Although small molecule acceptors based on PDI have been more widely used, some PDI-based copolymers have been also reported[26,27,28,29,30] giving promising results.

In this study, PDI was incorporated as an electron acceptor in a series of easily accessible, random terpolymers, of the "one donor – two acceptor" (D-A1)-(D-A2) type, synthesized via Suzuki polymerization. By combining the PDI group with benzothiadiazole electron acceptor group[31] and carbazole electron donating group in different ratios along one single polymer backbone, we anticipated to create PDI-based processable terpolymers with tunable electronic properties, broadened absorption and improved solubility. The 2,7-carbazole co-monomer was used as the donor comonomer with varying compositions of PDI and benzothiadiazole derivatives as the electron accepting moieties. Two different benzothiadiazole (BTZ) derivatives were employed, the di-thienyl substituted-BTZ, named TBTZ, and the di-3,4-ethylenedioxythienyl substituted-BTZ, named EDOTBTZ. The different benzothiadiazole derivatives and the varying ratios of the two acceptors were studied regarding their impact on the polymers' optical and electrochemical characteristics. The random terpolymers present broad

absorption profiles (300-700 nm), moderate bandgap (1.61 eV to 1.80 eV) and deep-lying HOMO/LUMO energy levels (-5.9 eV and -4.1 eV, respectively). It was found that the PDI molecule imposed stronger n-type character as its ratio increased, disrupting the co-planarity and improving the solubility of the final terpolymer.

Binary polymeric blends are becoming increasingly attractive platforms for the development of all-polymer solar cells. Despite the wide availability of polymeric donor derivatives today, a need has arisen for the identification of suitable electron accepting polymeric derivatives that can be incorporated in solution-processing protocols for the development of low-cost bulk heterojunction solar cells.

Under this aspect, in this first case study, the PDI-rich terpolymer P4, was blended with the well-known p-type polymer[32] PCE10 [poly([2,6′-4,8-di(5-ethylhexylthienyl)benzo[1,2-b;3,3-b]dithiophene]{3-fluoro-2[(2-ethylhexyl)carbonyl]thieno[3,4-b]thiophenediyl})] (E_{HOMO}= -5.40 eV, E_{LUMO}= -3.31 eV), in various ratios and used as the photoactive layer in bulk heterojunction photodiodes. Photodiode devices with PCE10:P4 active layers were fabricated both in conventional and inverted device configurations. The composition dependent charge photogeneration efficiency of the photodiodes was monitored by means of EQE measurements. Excitation intensity dependent measurements of the device short-circuit current and open-circuit

voltage were performed to identify the main charge recombination loss mechanism in these systems. The charge transport properties of the PCE10:P4 system was monitored based on single-carrier devices prepared with photoactive layers identical to those of the photodiode devices. For reference purposes, the charge transport properties of PCE10-only and P4-only devices were also studied.

2. Results and discussion

2.1 Synthesis of polymers.

The main focus of this work was to develop highly processable, random terpolymers of the "one donor – two acceptor" (D-A1)-(D-A2) type, from organic semiconducting building blocks that are easily accessible and synthetically versatile. The 2,7-carbazole monomer was selected as the donor component, due to its highly rigid conjugated structure, its chemical and environmental stability, along with its good charge transport properties. In order to afford highly soluble terpolymers, the dibromo-N-heptadecan-9-yl-carbazole (diBr-HD-carbazole) with the long heptadecanyl alkyl chain was employed and subsequently, the di-boronic ester-HD-carbazole was prepared in good yields through the standard two-steps procedure[33]. Regarding the electron acceptor units, in the first case the *N,N*-di-(2-ethylhexyl)-1,7/1,6-di-bromo perylene diimide was used, which is known for its strong n-type character. This was synthesized in a two-step procedure affording the final dibromo product in multigram scale[34]. In addition, the benzothiadiazole (BTZ) unit was employed, which has also gathered considerable attention for constructing donor-acceptor copolymers owing to its planar structure, its good electron accepting character and low-cost commercial availability[31]. Two different BTZ derivatives, the 4,7-di-(5-

bromothiophene-2-yl)-2,1,3-benzothiadiazole (diBr-thien-BTZ and the 4,7-di-(5-bromo-3,4-ethylenedioxythiophene-2-yl)-2,1,3-benzothiadiazole (diBr-EDOT-BTZ) were used as comonomers in the polymerizations. The incorporation of the EDOT unit was motivated by its strong electron rich character, which can enhance the p-type capacity, providing in some cases stronger "push-pull" effect and red-shifted absorbance[35,36].

The synthetic procedure for the random terpolymers is depicted in Scheme 1. The random terpolymers bearing carbazole, and various ratios of PDI and TBTZ are named P1-P5, while the terpolymers bearing carbazole, and various ratios of PDI and EDOTBTZ are named P6-P9.

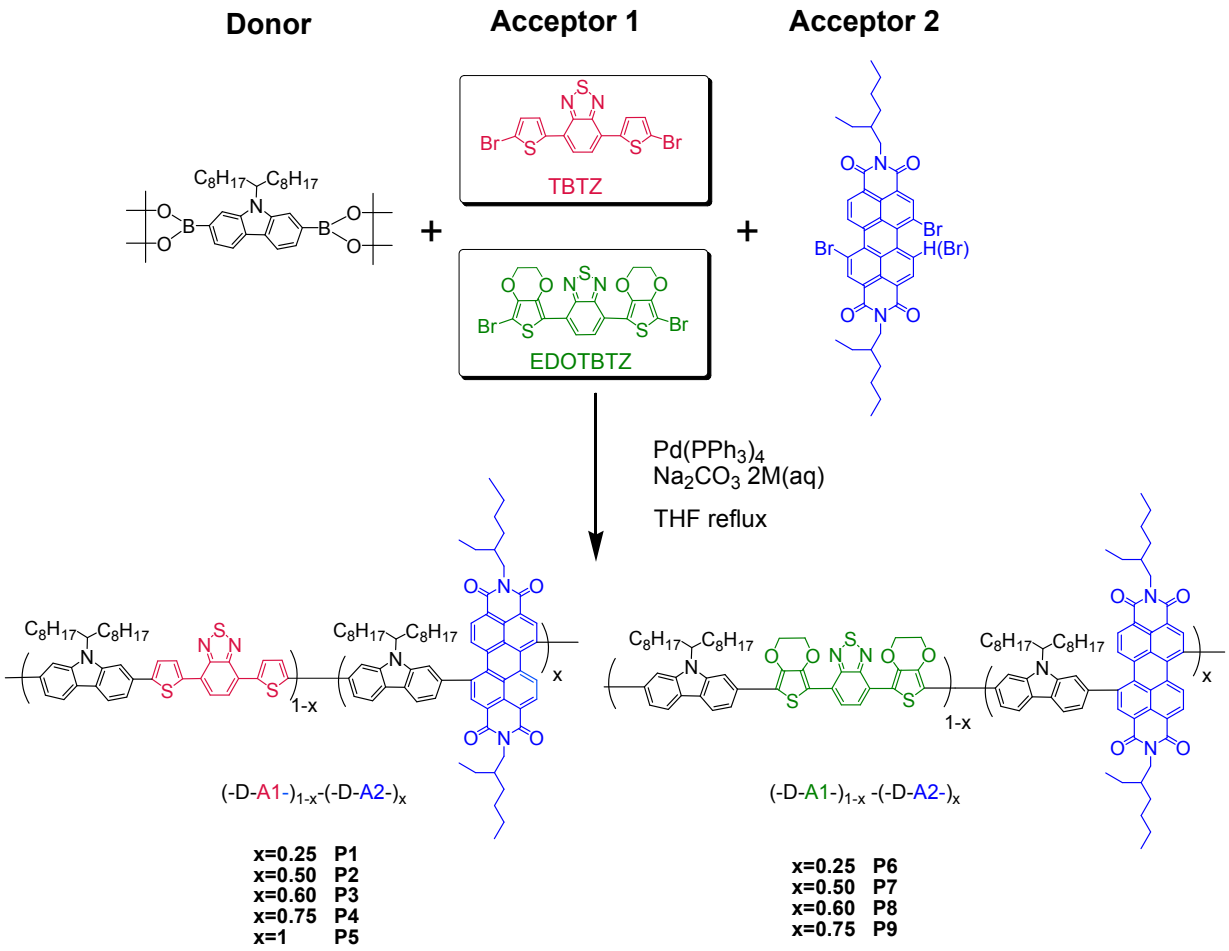

Scheme 1. Synthesis of P1-P9 random terpolymers with various ratio of PDI and BTZ groups by Suzuki polycondensation reaction.

Two different polymerization conditions were studied for the preparation of the terpolymers through palladium-catalyzed Suzuki polycondensation. Firstly, the reaction was performed using an aqueous solution of tetraethylammonium hydroxide 20% (Et_4NOH) as base, a procedure that has been reported and optimized for the synthesis of the low band-gap copolymer PCDTBT[37,38].

However, the obtained molecular weights were considerably low. Therefore, we changed to the more typical aqueous sodium carbonate solution as base which resulted in higher molecular weight polymers and therefore, it was maintained in all further polymerizations. Furthermore, using tetrahydrofuran as the solvent, instead of the commonly employed toluene, also led to higher molecular weights. At the last step of the polymerization reaction, phenylboronic acid and bromobenzene were added successively to the mixture, each followed by an additional 2 h heating at reflux for end-capping the polymer chains. Finally, all crude polymers were refluxed in acetone for at least 4 h in order to remove any unreacted monomers or oligomers. Better solubility was observed for the terpolymers based on the EDOTBTZ group that were all easily dissolved in chloroform. On the other hand, two of the terpolymers bearing the TBTZ unit, (P1 and P2), were only partially soluble in chloroform. Of these two TBTZ terpolymers, two different polymer fractions were thus obtained, a chloroform soluble fraction and an *o*-DCB one.

The chemical structure of the obtained polymers was verified via ^{1}H NMR spectroscopy and their molecular characteristics were determined using gel-permeation chromatography (GPC) in chloroform. The molecular weights of the terpolymers are given in Table 1, with M_n values ranging from ~8 kDa to ~19 kDa. It should be noticed that upon increasing the PDI content (see

also Figure S1), higher molecular weights were obtained. For the EDOTBTZ-based copolymers, when the ratio of PDI was 25%, namely the P6 terpolymer, the molecular weight obtained was as low as 6.5 kDa. On the contrary, the highest molecular weight of M_n = 11 kDa was obtained for the P9. An analogous behavior was noticed for the TBTZ-based terpolymers for which the highest molecular weight was obtained for the PDI-rich terpolymer P4 (M_n = 18 kDa).

Table 1. Feed ratios and GPC results of the terpolymers.

Terpolymer	Feed ratio X= -PDI	M_n[a,b]	M_w[a,b]	PD[a,b]
TBTZ based terpolymers				
P1[c]	0.25	9800	15700	1.6
P2[c]	0.50	12000	31200	2.37
P3	0.60	10800	24500	2.27
P4	0.75	18600	40300	2.17
Carbazole - PDI copolymer				
P5	1	15000	25000	1.70
EDOTBTZ based terpolymers				

P6	0.25	6500	10700	1,65
P7	0.50	7500	15000	2.00
P8	0.60	7800	13400	1.73
P9	0.75	11000	19000	1.74

a) as determined via GPC, using $CHCl_3$ as eluent, versus PS standards, at RT

b) M_n = number average molecular weight, M_w = weight average molecular weight, PD = polydispersity = M_w/M_n

c) GPC measurements were performed only for the $CHCl_3$ soluble fractions.

The structural composition of the terpolymers was evaluated by ^{1}H NMR (Figure 1 and Figure 2). In Figure 1, the ^{1}H NMR spectra (from 10.00 to 4.00 ppm) of P1-P5 terpolymers in $CDCl_3$ are presented. The signals corresponding to the methylene protons of the ethyl hexyl aliphatic chain of the PDI attached to the first carbon at the imide group are observed from 4.3 to 4.0 ppm. The characteristic peak attributed to the N-C*H* methine proton of the heptadecanyl chain of the carbazole unit is found at around 4.55 ppm and is shifted to 4.7 ppm with increasing the ratio of the BTZ. This downfield shift of the aliphatic signal may be attributed to steric effects. Typically, deshielding of protons is observed due to intramolecular steric interactions[39,40,41].Thus, we can assume that TBTZ imparts a more rigid and planar structure

compared to the PDI unit. The aromatic protons of the TBTZ group are detected from 7.7 to 7.6 ppm in all terpolymers, confirming the incorporation of the group to the final polymeric backbone. As expected, this proton signal was not observed in the ^{1}H NMR spectrum of the P5 copolymer due to the absence of the TBTZ, underlining the correct assignment of the peaks.

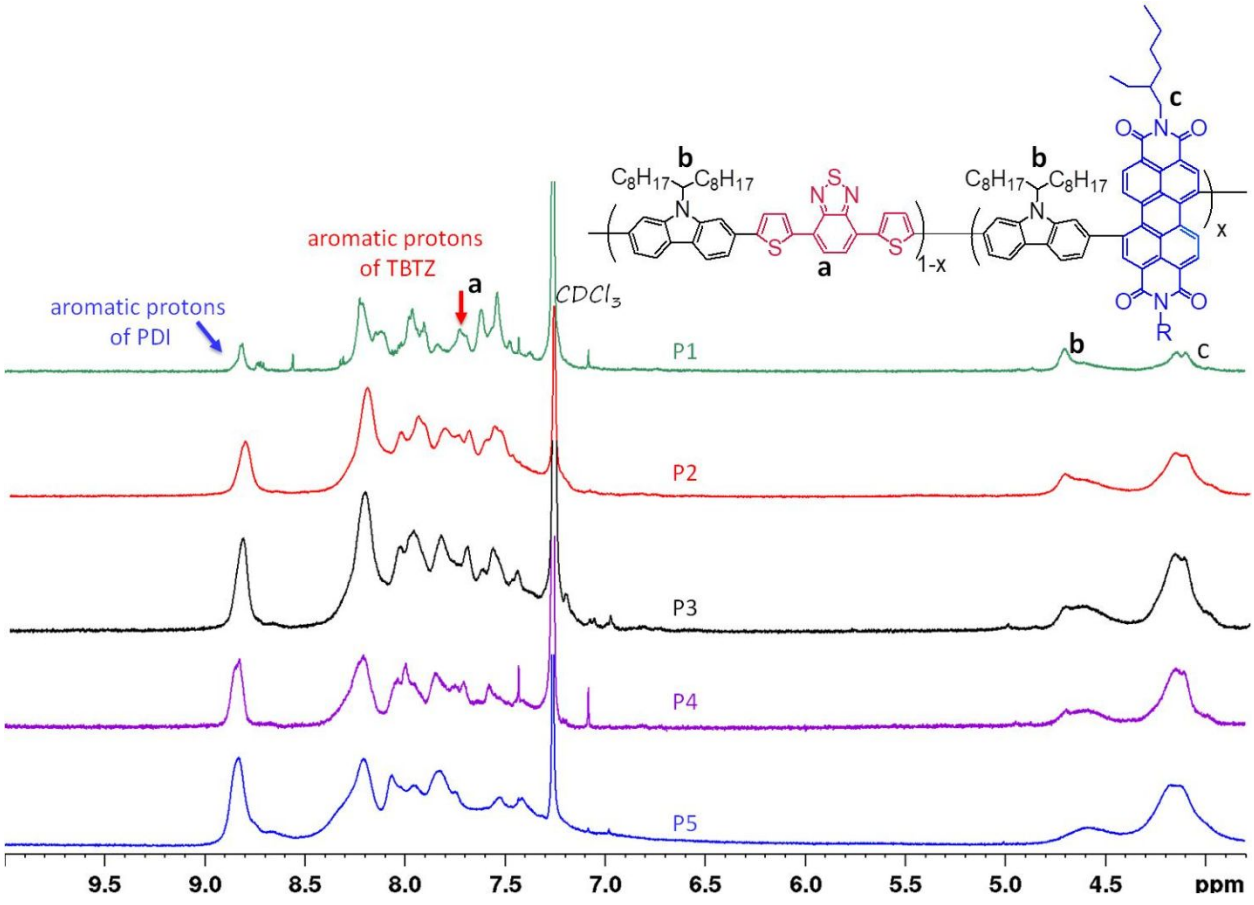

Figure 1. ^{1}H NMR spectra (from 10.00 to 4.00 ppm) of P1-P5 terpolymers in $CDCl_3$.

In Figure 2, the ^{1}H NMR spectra (from 10.00 to 4.00 ppm) of P5-P9 terpolymers in $CDCl_3$ are presented. The signals corresponding to the aliphatic chain of the PDI and the carbazole units are also observed here, presenting the same downfield shift as above mentioned. From 8.6 to 8.5 ppm a distinct peak is clearly observed in all the terpolymers' spectra, assigned to the aromatic protons of the EDOT-BTZ unit, that are absent in the spectrum of P5. Additionally, a new peak at 4.5 ppm is observed at the terpolymers' spectra which is attributed to the aliphatic protons of the EDOT group. This peak becomes more prominent with increasing the ratio of the EDOT-BTZ group along the final polymeric backbone, confirming the successful incorporation of the EDOT moiety.

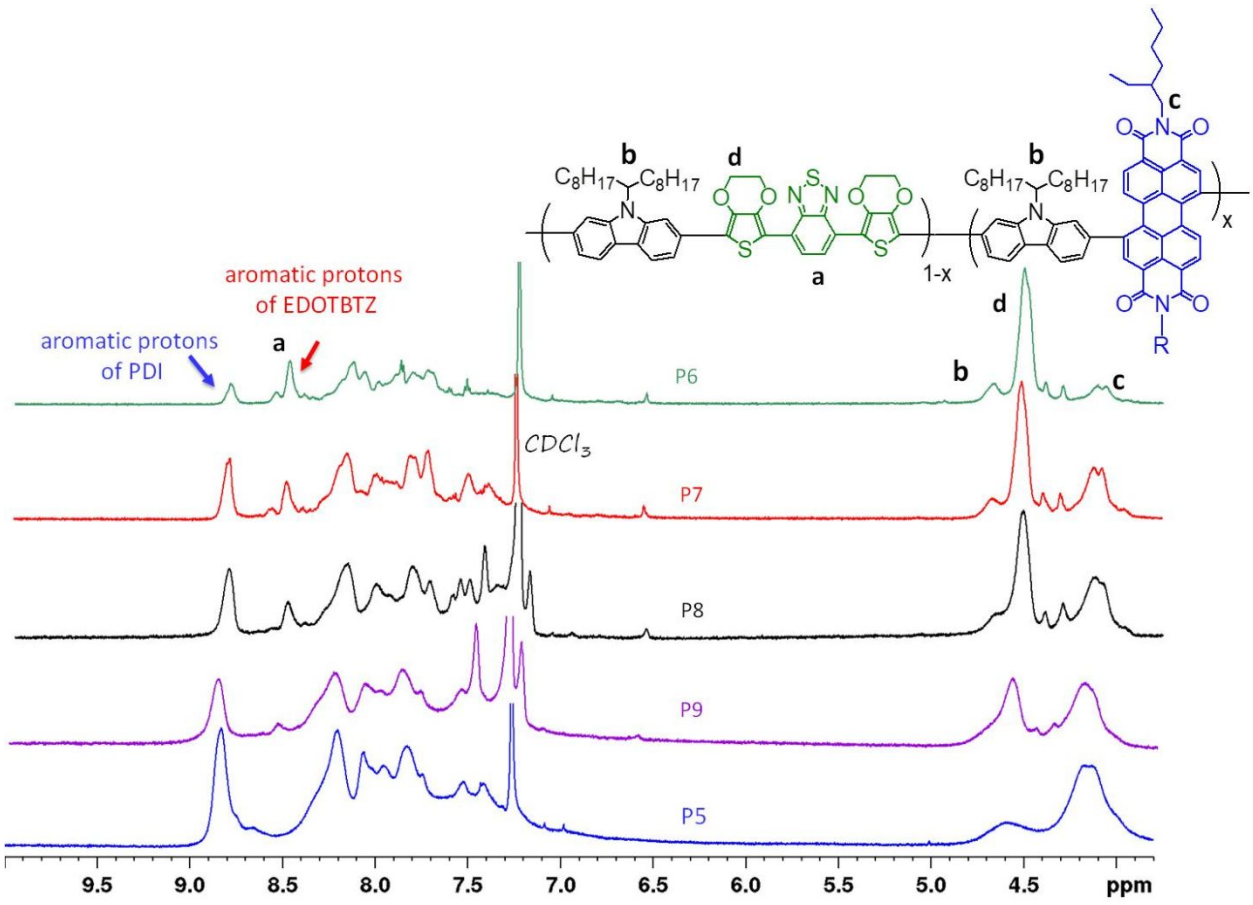

Figure 2. ^{1}H NMR spectra (from 10.00 to 4.00 ppm) of P5-P9 terpolymers in $CDCl_3$.

From the integration of the assigned protons, the percentage of each unit (carbazole, PDI and the two different types of the BTZ unit) in the final polymeric backbone was calculated (see Table 2). The feed ratios of the monomers BTZ:PDI (%mol) used in the polymerizations are in good agreement to the ratios of the moieties estimated via ^{1}H NMR, revealing that the composition in the final terpolymers can be indeed controlled and fine-tuned via this synthetic methodology.

Furthermore, thermogravimetric analysis (TGA) of the terpolymers revealed that all terpolymers possess good thermal stability with degradation temperatures above 450 °C (5% weight loss) under nitrogen, as shown in Figure S2, which is an important aspect of such polymers applicability in devices exposed to real operating conditions[42].

Table 2. Monomer Feed ratio of BTZ and PDI units and BTZ:PDI final ratio (mol%) estimated by ^{1}H NMR.

Copolymers	BTZ:PDI (mol%) Monomer Feed	BTZ PDI: (mol%) Peak Area from 1H NMR
***TBTZ* based terpolymers**		
P1	75:25	57:43
P2	50:50	48:52
P3	40:60	40:60
P4	25:75	23:77
Carbazole - PDI copolymer		
P5	100:0	100:0
***EDOTBTZ* based terpolymers**		

P6	75:25	70: 30
P7	50:50	45:55
P8	40:60	35:65
P9	25:75	22:78

2.2 Optical and Electrochemical Investigation

The optical properties of the synthesized terpolymers were evaluated using UV-Vis and PL spectroscopies. The terpolymers were studied in ortho-dichlorobenzene (*o*-DCB) solutions and in solid state by preparing thin films using the drop casting method. The optical band gaps were determined based on the absorption onsets using equation (5) (see Experimental Part in the Sup. Info. section).

In Figure 3a, the UV-Vis spectra of P1-P5 terpolymers in *o*-DCB solutions are presented. Two strong absorption bands, typical for donor-acceptor copolymers coexist in every spectrum. In the shorter wavelengths an absorption peak owing to π-π* transitions appears, which is red-shifted as the ratio of the TBTZ increases and specifically for the P3 terpolymer, a broader absorption profile covering the full range from 300 to 400 nm is achieved. At higher wavelengths (from 400

to 700 nm) a second absorbance is evident due to intramolecular charge transfer (CT) processes among the comonomers. Terpolymers having more TBTZ (>40%) exhibit more intense CT absorption bands, compared to the terpolymers with higher PDI content. This phenomenon can be explained from an induced tilt in the polymer backbone due to the loss of planarity that the large perylene core imposes[43,44]. The same trend is also observed in the absorption spectra of the terpolymers in film form (Figure 3b), with the more intense CT band observed for the P1 terpolymer. Typically, all terpolymers showed broader absorption profiles in film form compared to their solutions, with absorption tails reaching up to ~700nm.

The optical properties of P5-P9 terpolymers in *o*-DCB solutions are presented in Figure 3c. The absorption peak between 300 – 400 nm arising from π-π* transitions is also affected by the EDOTBTZ:PDI ratio. With increasing of the EDOTBTZ component, the peak at 390 nm becomes more intense. For the P7 and P8 terpolymers, two bands at 330 and 390 nm coexist, leading to broader absorbance profiles. In higher wavelengths, the CT band found in the range of 450 and 700 nm becomes more intense as the EDOTBTZ content increases, following the same trend as for the TBTZ bearing terpolymers. In film form (Figure 3d), as the EDOTBTZ component increases, the absorbance is red-shifted indicating stronger interchain packing in the

solid state, owing to the more planar structure of EDOTBTZ that imparts more ordered structures to the final terpolymers. For the P6 terpolymer, two maxima due to the CT process are noticed, located at 600 nm.

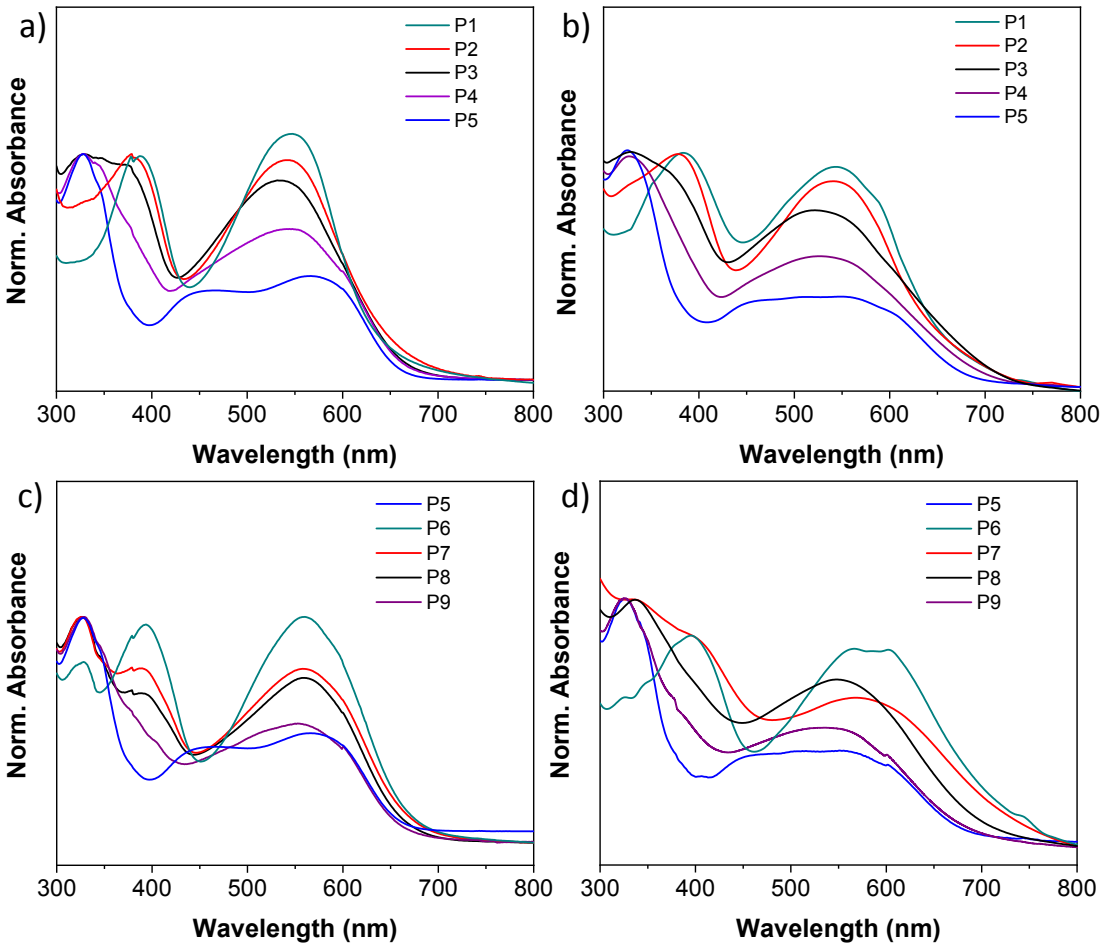

Figure 3. Normalized UV-Vis spectra of P1-P5 terpolymers a) in *o*-DCB solutions and b) in film form; of P5-P9 terpolymers c) in *o*-DCB solutions and d) in film form.

From the PL spectra of all terpolymers in *o*-DCB solutions and in film form (Figure S3), it is evident that all polymers are red emitters with emission peaks between 600 and 750 nm (λ_{max} from 580 to 632 nm). The P5 copolymer shows an emission with λmax at 664 nm both in solution and in film. With the reduction of the percentage of PDI, blue shifted emissions are observed in solution. Notably, for the P3 a featureless spectrum was detected, where neither BTZ nor PDI emit. The terpolymers present red shifted emission in film form compared to their solutions with a difference of 75 nm approximately (λ_{max} = 690nm). The EDOTBTZ based terpolymers solutions presented similar photoluminescence behavior to the TBTZ terpolymers with PL ranging from 600-650 nm. For this case, as the PDI content decreases, the emission in solution is blue shifted and for the P7 and P8 an almost complete quenching of fluorescence emission is observed. Moreover, for all EDOTBTZ-based terpolymers no fluorescence emission is noticed in film form, which can be attributed to increased interchain aggregation in the solid state[45].

The electrochemical properties of all synthesized terpolymers were investigated via cyclic voltammetry (CV). The reduction and oxidation onset potentials and the calculated LUMO and HOMO levels are detailed in Table 3, together with the optical properties. In Figure 4, the cyclic

voltammograms of the terpolymers are provided. The highest occupied molecular orbital (HOMO) and lowest unoccupied molecular orbital (LUMO) energy levels were estimated by combining both absorption spectroscopy and CV. Drop-cast films of the terpolymers in acetonitrile were used for the cyclic voltammetry analysis. We should point that CV measurements can have errors of over ±0.1 eV, particularly when thin films of the materials are deposited onto the working electrode, as is our case[46]. For materials based on the PDI block that presents strong n-type characteristics, HOMO levels are usually estimated from the E_g^{opt}. Taking these into consideration, the LUMO energy levels were calculated from the first reduction onset potential. The HOMO energy levels were estimated both from the oxidation onset potentials and from the LUMO levels and the optical bandgap (E_g^{opt}) using the equation:

E_g^{opt}= HOMO-LUMO [eV]

For the TBTZ based terpolymers P1-P4, upon increasing the PDI-content, the LUMO level decreases with LUMO levels ranging from -3.7 to -4.0 eV. An analogue behavior was noticed for the HOMO levels calculated from the oxidation potential. The HOMO levels calculated from oxidation onset potentials are located between -5.99 and -6.12 eV. Adding the LUMO values to the $E_g^{opt}$the HOMO levels follow the same trend and are found between -5.30 and -5.87 eV. For

the EDOTBTZ based terpolymers P6-P9, lower optical bandgaps were found due to a stronger 'push-pull' effect of the EDOTBTZ moiety. The LUMO levels did not present considerable differences concluding that they are mainly affected by the PDI component. The two electron donating oxygen moieties of EDOT are known to increase the electron donating ability[47] and therefore higher-lying HOMO levels were detected compared to the TBTZ based terpolymers.

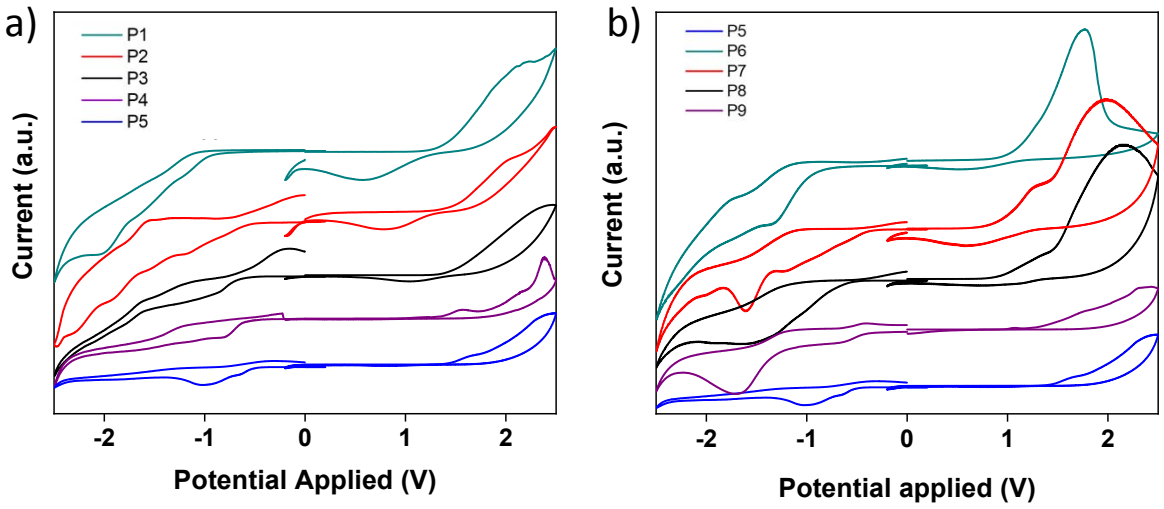

Figure 4. Cyclic voltammograms spectra of (a) P1-P5 and (b) P5-P9 terpolymers.

Table 3. Absorption and Electrochemical Properties of the synthesized terpolymers.

	λ (nm)			E_g^{opt} (eV)	E_{on}^{RED} (V)	E_{on}^{ox} (V)	E_{LUMO} (eV)	E_{HOMO} (eV) from E_g^{opt}	E_{HOMO} (eV) from E_{on}^{ox}
	Sol	*film*	*onset*						
***TBTZ* based terpolymers**									
P1	550	550	715	1.73	-0.94	1.37	-3.71	-5.29	-6.02
P2	543	545	710	1.75	-0.70	1.44	-3.95	-5.78	-6.09
P3	538	530	700	1.77	-0.64	1.45	-4.01	-5.84	-6.10
P4	550	528	700	1.77	-0.61	1.37	-4.04	-5.87	-6.02
Carbazole - PDI copolymer									
P5	565	560	690	1.80	-0.57	1.43	-4.08	-5.88	-6.08
***EDOTBTZ* based terpolymers**									
P6	560	600	770	1.61	-0.97	1.13	-3.68	-5.29	-5.78
P7	560	570	760	1.63	-0.50	0.88	-4.15	-5.78	-5.53
P8	560	550	720	1.72	-0.65	0.90	-4.00	-5.72	-5.55
P9	550	540	710	1.75	-0.55	1.36	-4.10	-5.85	-6.01

2.3 Photodiode Characterization

The herein presented PDI-based terpolymers constitute an interesting case study of electron acceptors for all polymer BHJ photodiodes. For this scope a representative terpolymer from the above terpolymers library, selected for its high molecular weight and its high PDI content, was further studied in BHJ-photodiodes, wherein the PCE10 polymer was used as an electron donor. A set of PCE10: P4 ratios was prepared and the ratio dependent response of the photodiode devices was monitored. Based on the cyclic voltammetry results (Table 3), the P4 derivative is a suitable n-type component to match with the PCE10 polymer donor for facilitating charge photogeneration. The energy levels of PCE10 are appropriate for forming a type-II bulk heterojunction with P4 that favours both processes of light-induced electron and hole transfer between the two materials.

First, the UV-Vis absorption spectra of the single-component films of the two polymers were recorded, when deposited onto pre-cleaned fused silica quartz substrates. As displayed in Figure 5a below, the two materials exhibit complementary absorption profiles; P4 absorbs light across the UV-Vis range, whereas PCE10 exhibits additional light absorbing power beyond 700 nm. The absorption profiles of the PCE10: P4 blends are presented in Figure 5b for the three ratios of 1:1, 1:2 and 1:3. In all cases, the composite films exhibit a broad absorption across the 350-800

nm spectral range and their relative absorption strength at 550 nm increases as the P4 content in the blend is increased.

AFM imaging was employed for monitoring the surface topography of these blends and the miscibility of the two polymers as a function of their ratio is depicted in Figure 5c. For reference purposes, the surface topography of the PCE10-only and P4-only films were also examined. Both polymers form very smooth films with low root mean square roughness (RMS = 1 nm). In regard to the binary blend systems, as the P4 content increases, the films surface becomes more homogeneous and smoother, depicting a better miscibility between the two polymeric materials.

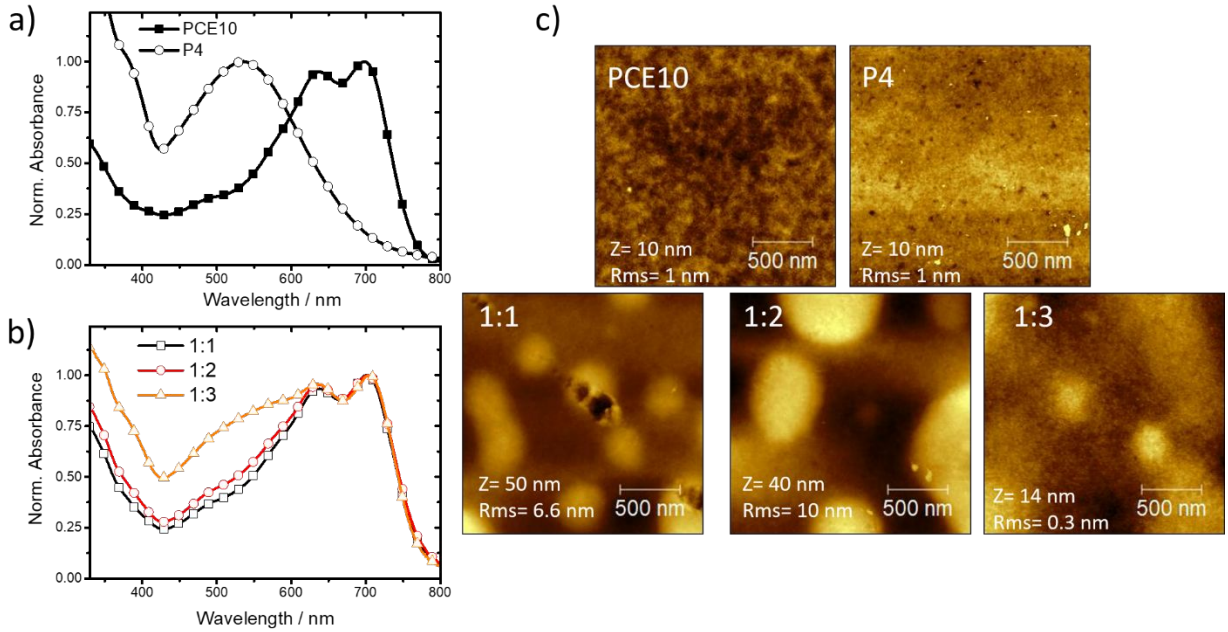

Figure 5. a) Normalized absorption spectra of b) the neat components and c) the PCE10: P4 blend films with 1:1, 1:2 and 1:3 ratios, d) tapping mode atomic force micrographs of films with PCE10-only, P4-only and PCE10: P4 blends with different ratios. All films were deposited on fused silica quartz substrates from *o*-dichlorobenzene.

The photodiode response of the PCE10: P4 photoactive layer was studied both in conventional and inverted device geometries with glass/ITO/PEDOT:PSS and glass/ITO/ZnO bottom electrodes, respectively. The frontier orbital alignment for each device geometry and its corresponding polarity are displayed in Figure S4.

The photocurrent generation efficiency of the fabricated devices was studied by means of EQE measurements as a function of the blend composition. Figure 6a and Figure 6b present the obtained EQE spectra of these devices.

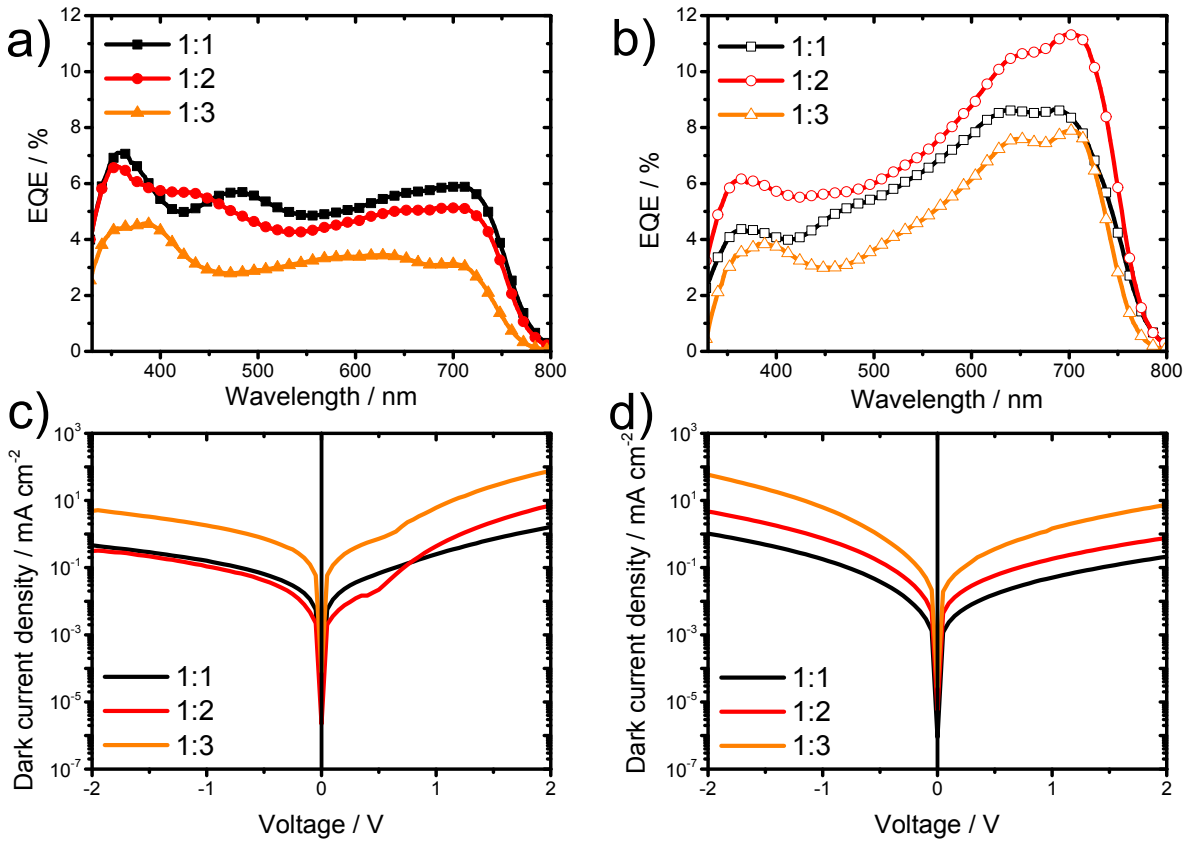

Figure 6. External quantum efficiency (EQE) spectra of the photodiode devices with a) conventional and b) inverted device geometries, as developed by PCE10: P4 photoactive layers with different blend composition. Composition dependent dark J-V curves of photodiode devices with c) conventional and d) inverted device geometries. In all cases, devices with photoactive

layers of 1:1, 1:2 and 1:3 compositions correspond to black, red and orange color codes, respectively.

In all cases, the efficiency of the conventional PCE10: P4 devices is lower than their inverted device analogues. For the case of the conventional device structures, the EQE progressively drops as the P4 content in the blend increases. In the 700 – 800 nm spectral range, the conventional PCE10: P4 devices exhibit a poor light-to-current conversion efficiency, regardless of their photoactive layer blend composition. This could be attributed to a low dissociation efficiency of the excitons formed in the PCE10 component[48] or to monomolecular charge recombination losses[49] at short-circuit conditions. Upon translating the PCE10: P4 system to the inverted device structure, the obtained EQE spectra are in good agreement with the absorption spectra of the blend. As shown in Figure 6b, the inverted device of the 1:2 composition delivers a maximum EQE at 698 nm reaching to 11%. Integration of the EQE spectrum of this system with the AM1.5G solar spectrum projects to the generation of 2.03 mA cm^{-2} photocurrent density. The discrepancy between the EQE response of the two device types that share the same photoactive layer, most likely is a result of the different surface energy of the PEDOT:PSS and the ZnO electrodes. Previous studies on PDI-based photodiode devices have shown how the electron-transporting quadropolar PDI component preferentially segregates towards the hydrophilic PEDOT:PSS layer, thereby impeding the extraction of photogenerated electron to the electron-collecting electrode of devices with conventional geometry[50].

Figure 6c and Figure 6d presents the dark current density J-V curves of the fabricated photodiodes. In both set of devices, an increase of the dark current takes place as the P4 content of the device layer increases. However, the inverted devices exhibit up to 15 times higher dark current at reverse bias operation, most likely due to the injection of holes from the ZnO electrode (φ_{ZnO} = 4.4 eV) to the HOMO levels of the PCE10 and P4 materials. For the conventional (inverted) device types, forward dc bias direction J-V measurements were enabled by positively biasing the glass/ITO/PEDOT:PSS (Au) hole-collecting electrode, in respect to the Ca/Al (glass/ITO/ZnO) electron-collecting electrode. At -2V reverse bias, the 1:1, 1:2 and 1:3 conventional devices exhibit a dark current density of 0.46 mA/cm^2, 0.31 mA/cm^2 and 4.90 mA/cm^2 respectively. The current rectification factor between ± 2V for these systems is found to be 3.5, 23 and 15.5. By inverting the device geometry, the diode-like character of the system is degraded and the dark current density is increased. At reverse bias operation of -2V, the dark current density of the inverted devices with the 1:1, 1:2 and 1:3 blends becomes 1.04 mA/cm^2, 4.71 mA/cm^2 and 58.37 mA/cm^2, respectively. For these systems, the corresponding current rectification factor between ± 2V reduces significantly to 0.20, 0.16 and 0.12.

The photoresponse of the fabricated PCE10: **P4** photodiodes was studied further as a function of the incoming photoexcitation power (P_{exc}). A 532 nm DPSS CW laser source was used for photoexciting the devices at progressively increased powers in the range between 0.25 – 60 mW. For each device system a set of power-dependent J-V curves were registered. Figure 7a and

Figure 7b presents the short-circuit current density J_{sc} of the studied systems as a function of P_{exc}. Both conventional and inverted device geometries exhibit a nearly linear dependence of J_{sc} on P_{exc} that can be described by the $J_{sc} \propto P_{exc}^{\alpha}$ functional with the α exponent value kept close to 1. The observed linearity of J_{sc} on photoexcitation intensity indicates that no space charge effects are limiting the photocurrent of the studied device structures[51]. It has been suggested that electron transport in the class of organic semiconductors is limited by electron trapping sites formed by hydrated oxygen complexes[22] that have an energy of -3.6 – -3.8 eV[23]. Given the deep LUMO energy (E_{LUMO} = -4.08 eV, Table 3) of the n-type P4 terpolymer the performance of the P4-based photodiodes should not suffer from non-geminate charge recombination losses and a trap-free electron transport is expected in the PCE10:P4 devices. In order to verify this, we monitored the open-circuit voltage (V_{oc}) dependence of the photodiodes on P_{exc}.

With increasing power, the charge generation rate in the device photoactive layer increases, thereby leading to the increase of the device V_{oc} parameter according to the $V_{oc} \propto \beta \times \frac{kT}{q} \ln(P_{exc})$ functional. Ideally, when only bimolecular recombination losses are operative, the β coefficient is equal to unity[52]. As shown in Figure 7c and Figure 7d, conventional devices exhibit higher V_{oc} in the excess of the P4 component in the photoactive layer. Both conventional and inverted

device structures exhibit values of $\beta = 2$ when the blend ratio is kept at 1:1, which suggests that non-geminate recombination channels are present in the PCE10:P4 photoactive layer. Moreover, non-geminate recombination losses become more important as the content of the P4 component in the blend increases. This manifests in the stronger dependence of V_{oc} on photoexcitation power that is observed for the devices of the 1:2 and 1:3 photoactive layers. One interpretation could be that with increasing the P4 terpolymer content the concentration of electron trap sites in the blend increases. However, the energy of the traps must be equal or higher than the LUMO energy of P4, so the formation of hydrated oxygen complexes[23] cannot explain the origin of these electron trapping sites. Similar effects of substantial non-geminate charge recombination losses were reported previously for PDI-based OPV devices made by molecular PDI derivatives of equally deep LUMO energies[53]. It is likely that the electron traps identified in both P4 and the previously studied molecular PDI electron acceptors have a common source. In the P4 specifically, they could be the result of nanograin sites formed by the packing of the PDI co-monomer in the PCE10: P4 photoactive layers. The attachment of bulky substituents on the imide sites of the PDI co-monomer should hinder the PDI side-chain segregation of adjacent P4 polymer backbones, thereby preventing the formation of aggregates at the nanoscale. At present,

the acquired AFM images provide no evidence in support of aggregate formation in the PCE10:P4 blends.

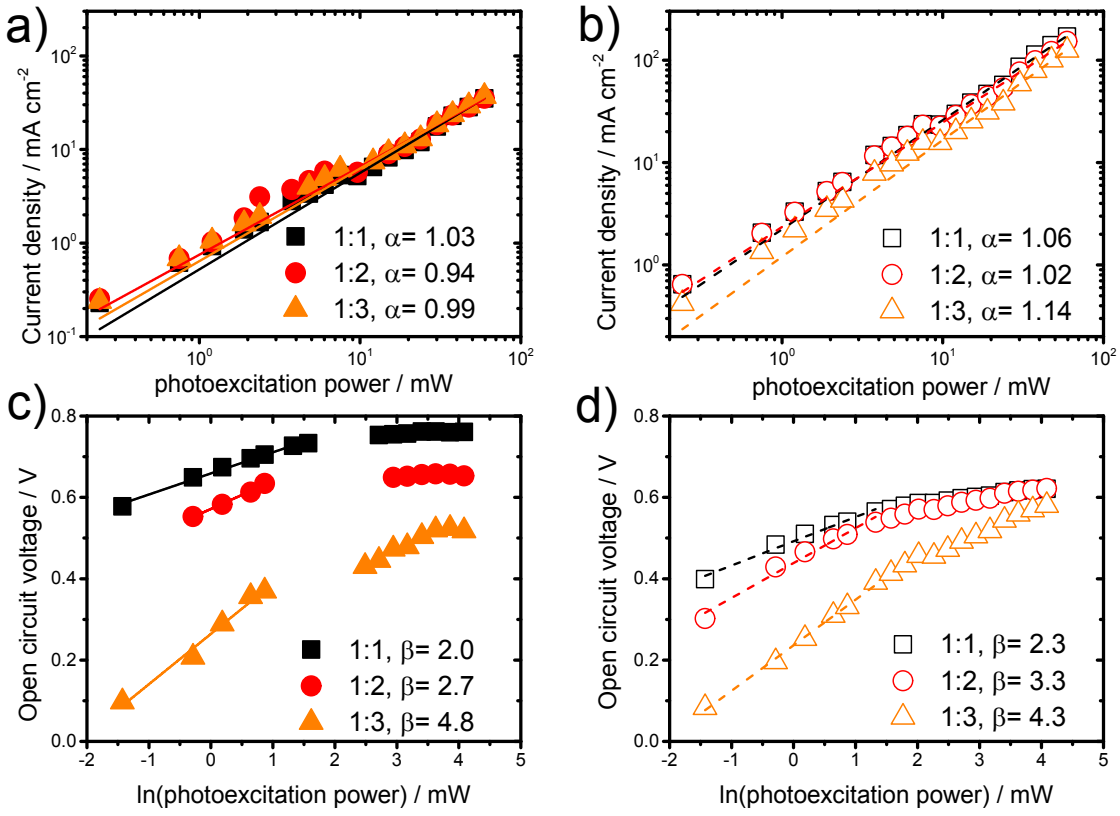

Figure 7. Photoexcitation dependent short-circuit current density of PCE10:P4 photodiode devices with a) conventional and b) inverted device geometries. Photoexcitation dependent open-circuit voltage of PCE10:P4 photodiode devices with c) conventional and d) inverted device geometries. In all cases the different PCE10:P4 blend compositions of 1:1, 1:2 and 1:3

correspond to black, red and orange color codes. Solid lines in (a), (b) and dash lined in (c), (d) correspond to fits on the experimental data based on the functionals described in the main text.

2.4 Charge Transport Properties

The charge-transport properties of the PCE10:P4 blends were examined. Spin-coated PCE10:P4 films were used as active layers in unipolar carrier device geometries. The zero-field values of hole- ($\mu_{0(h)}$) and electron- ($\mu_{0(e)}$) mobilities of these devices were deduced by the dark J−V curves based on the equation [54] $J(V) = \frac{9}{8}\varepsilon_0\varepsilon_r\mu_0\frac{V^2}{L^3}e^{0.89\beta\sqrt{\frac{V}{L}}}$

Identical measurements were performed for single-carrier devices of the PCE10:P4 blend films with different blending ratios. For each material combination, a set of dark J-V curves was collected for devices developed by the same solution and fabricated on the same device fabrication round. For the obtained dark J-V data sets, the mean zero field carrier mobility was calculated for each system together with its corresponding standard deviation. Figure 8 presents the composition dependent zero-field mobility values for holes and electrons.

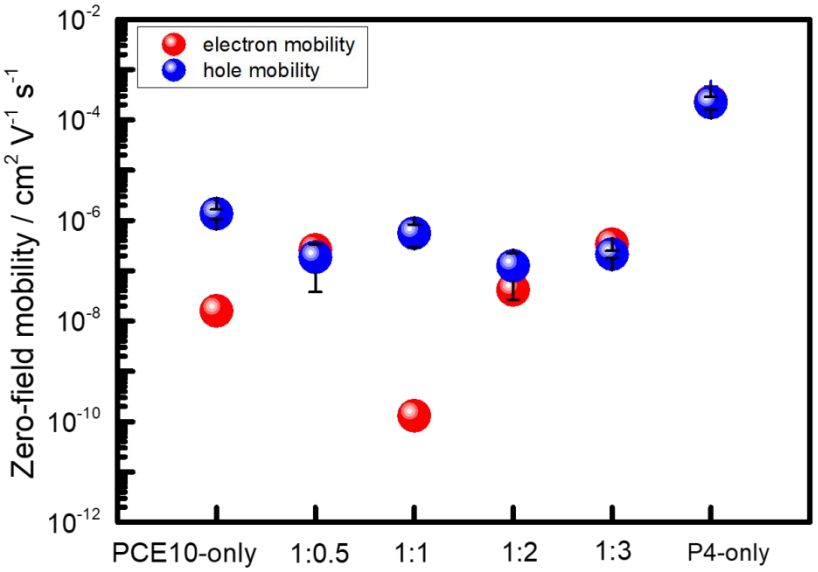

Figure 8. Composition dependent, zero-field carrier mobility values of electrons (red symbols) and holes (blue symbols) as derived by SCLC measurements of unipolar PCE10:P4 devices.

Interestingly, the P4 material is found to exhibit higher electron and hole mobility values than those found for PCE10. Mixing P4 with PCE10 leads to much lower carrier mobility values. However, charge transport in the PCE10:P4 photoactive layer remains balanced so long the 1:1 blend ratio is avoided. Remarkably, the electron and hole mobility values of the P4-only devices are found to be comparable, suggesting the potential applicability of the P4 terpolymer as a material for field-effect transistor devices. Presumably, in the spin-coated P4 terpolymer film, both types of building blocks for hole (carbazole) and electron (perylene diimide, benzothiazole) transport adapt well-organized packing motifs.

3. Conclusions

A series of "one donor–two acceptor" (D–A1)-(D–A2) random solution processable terpolymers containing the accessible organic building blocks of carbazole, perylene diimide and two different substituted benzothiazole derivatives (di-thienyl, TBTZ, and di-3,4-ethylenedioxythienyl, EDOTBTZ) were developed. Different ratios of the co-monomers were used to manipulate backbone coplanarity and optoelectronic properties. It was found that, the wavelength and the intensity of the intramolecular charge transfer peak was tuned based on the ratio of the two acceptors (BTZ and PDI). The EDOTBTZ-based terpolymers present redshifted absorption and smaller bandgaps due to a more pronounced 'push-pull' effect and more rigid polymeric structure. The introduction of PDI reduces the LUMO level, whereas the EDOTBTZ unit affords higher-lying HOMO levels. The PDI-rich terpolymer, P4, was tested as an electron acceptor component in bulk heterojunction devices blended with PCE10. Photodiodes with PCE10:P4 active layers were studied in a range of blend compositions, both in conventional and inverted device configurations. The 1:2 blend ratio exhibited the optimum photocurrent generation efficiency in the inverted device structure. Both types of conventional and inverted PCE10:P4 photodiodes suffered from severe non-geminate charge recombination losses as

suggested by the dependence of the device open-circuit voltage on photoexcitation intensity. In regard to the charge transport properties of the P4 derivative alone, an ambipolar behavior was observed with hole and electron mobility values of 2.2 $\times 10^{-4}$ $cm^2V^{-1}s^{-1}$ and 6.3 $\times 10^{-5}$ $cm^2V^{-1}s^{-1}$, respectively. Upon blending P4 with PCE10 charge transport deteriorates. The elucidation of microstructure in these materials will disclose the nature of the electron trapping sites in their solid-state films, and contribute in the establishment of rigorous processing protocols for optimized charge transport suitable for all-polymer based blend systems.

Supporting Information

The following files are available free of charge. Materials and methods, synthetic procedures, characterization methods and additional characterization such as GPC analysis, Thermogravimetric analysis and PL spectra of the synthesized random terpolymers together with composition dependent dark J-V metrics of single-carrier devices.

Corresponding Authors

Email: p.keivanidis@cut.ac.cy

Email: andreopo@upatras.gr

Present Addresses

† Stefania Aivali − Département de Chimie, Université Laval, Québec G1V 0A6, Canada

§ Peisen Yuan − CIC nanoGUNE (Nanoscience Cooperative Research Center), San Sebastian, Donostia, 20018, Spain

Author Contributions

The manuscript was written through contributions of all authors. S.A. and P. Y. have contributed equally on this work. All authors have given approval to the final version of the manuscript.

Funding Sources

S.A. was financially supported by General Secretariat for Research and Technology (GSRT) and the Hellenic Foundation for Research and Innovation (H.F.R.I) Code:2358. J.D, D.G.G. and T.P. acknowledge the support of EPSRC Programme Grant FORTE (EP/R024642/1) and the RAEng Chair in Emerging Technologies (CiET1819/2/93).

4. References